Biochimica et Biophysica Acta 1847 (2015) 162–170

Contents lists available at ScienceDirect

Biochimica et Biophysica Acta

journal homepage: www.elsevier.com/locate/bbabio

Structural differences of oxidized iron–sulfur and nickel–iron cofactors in O_2-tolerant and O_2-sensitive hydrogenases studied by X-ray absorption spectroscopy

Kajsa G.V. Sigfridsson [a,1], Nils Leidel [a], Oliver Sanganas [a], Petko Chernev [a], Oliver Lenz [b], Ki-Seok Yoon [c,2], Hirofumi Nishihara [c], Alison Parkin [d,3], Fraser A. Armstrong [d], Sébastien Dementin [e], Marc Rousset [e], Antonio L. De Lacey [f], Michael Haumann [a,*]

[a] Freie Universität Berlin, Institut für Experimentalphysik, 14195 Berlin, Germany
[b] Humboldt-Universität zu Berlin, Mikrobiologie, 10115 Berlin, Germany
[c] Ibaraki University, Department of Bioresource Science, Ibaraki 300-0393, Japan
[d] University of Oxford, Department of Inorganic Chemistry, Oxford OX1 3QR, UK
[e] CNRS Marseille, Unité de Bioénergétique et Ingénierie des Protéines, 13402 Marseille, France
[f] Instituto de Catálisis (CSIC), 28049 Madrid, Spain

ARTICLE INFO

Article history:
Received 2 April 2014
Received in revised form 6 June 2014
Accepted 16 June 2014
Available online 12 October 2014

Keywords:
[NiFe]-hydrogenase
O_2-tolerance
FeS cluster
[NiFe] active site
X-ray absorption spectroscopy

ABSTRACT

The class of [NiFe]-hydrogenases comprises oxygen-sensitive periplasmic (PH) and oxygen-tolerant membrane-bound (MBH) enzymes. For three PHs and four MBHs from six bacterial species, structural features of the nickel–iron active site of hydrogen turnover and of the iron–sulfur clusters functioning in electron transfer were determined using X-ray absorption spectroscopy (XAS). Fe-XAS indicated surplus oxidized iron and a lower number of ~2.7 Å Fe–Fe distances plus additional shorter and longer distances in the oxidized MBHs compared to the oxidized PHs. This supported a double-oxidized and modified proximal FeS cluster in all MBHs with an apparent trimer-plus-monomer arrangement of its four iron atoms, in agreement with crystal data showing a [4Fe3S] cluster instead of a [4Fe4S] cubane as in the PHs. Ni-XAS indicated coordination of the nickel by the thiol group sulfurs of four conserved cysteines and at least one iron–oxygen bond in both MBH and PH proteins. Structural differences of the oxidized inactive [NiFe] cofactor of MBHs in the Ni-B state compared to PHs in the Ni–A state included a ~0.05 Å longer Ni-O bond, a two times larger spread of the Ni–S bond lengths, and a ~0.1 Å shorter Ni–Fe distance. The modified proximal [4Fe3S] cluster, weaker binding of the Ni–Fe bridging oxygen species, and an altered localization of reduced oxygen species at the active site may each contribute to O_2 tolerance.

1. Introduction

Hydrogenases (H_2ases) are enzymes which catalyze effective and reversible hydrogen (H_2) formation or cleavage at protein-bound metal centres [1–3]. They are of high interest in the contexts of renewable energy generation, biotechnology, and chemical catalysis. An obstacle for using H_2ases in applications is the rapid inactivation of many enzymes by oxygen (O_2) [4,5]. However, H_2ases from various bacterial species have been identified, which exhibit high O_2-tolerance of their H_2-turnover activity [6–9]. Understanding this unusual catalytic behaviour may lead to improved enzymes as well as to novel synthetic catalysts.

The known O_2-tolerant H_2ases all belong to the [NiFe] type, meaning that their active site contains one nickel and one iron atom [10]. In particular, members of the phylogenetically related subclass of O_2-tolerant membrane-bound [NiFe]-H_2ases (MBHs) have attracted much research effort [11–13]. They consist of a large subunit binding the [NiFe] active site of H_2 turnover and a small subunit with three iron–sulfur clusters in proximal, medial, and distal positions to the [NiFe] site, functioning as an electron transfer relay, and which are anchored to the periplasmic side of the cytoplasmic membrane via a *b*-type cytochrome. The standard type of O_2-inhibited periplasmic [NiFe]-H_2ases (PHs) shows similar subunits and cofactor complements, but a soluble cytochrome-*c* is the electron transfer partner in many cases (Fig. 1). Hydrogenase II

Abbreviations: EPR, electron paramagnetic resonance spectroscopy; EXAFS, extended X-ray absorption fine structure; FTIR, Fourier-transform infrared spectroscopy; H_2ase, hydrogenase; MBH, membrane-bound [NiFe] H_2ase; PH, periplasmic [NiFe]-H_2ase; TXRF, total-reflection X-ray fluorescence analysis; XANES, X-ray absorption near edge structure; XAS, X-ray absorption spectroscopy

* Corresponding author at: Freie Universität Berlin, FB Physik, Arnimallee 14, 14195 Berlin, Germany. Tel.: +49 30 838 56101; fax: +49 30 838 56299.
E-mail address: michael.haumann@fu-berlin.de (M. Haumann).
[1] Present address: MAX IV Laboratory, Lund University, 22100 Lund, Sweden.
[2] Present address: Kyushu University, International Institute for Carbon-Neutral Energy Research, Fukuoka 819-0395, Japan.
[3] Present address: University of York, Department of Chemistry, York YO10 5DD, UK.

http://dx.doi.org/10.1016/j.bbabio.2014.06.011
0005-2728/

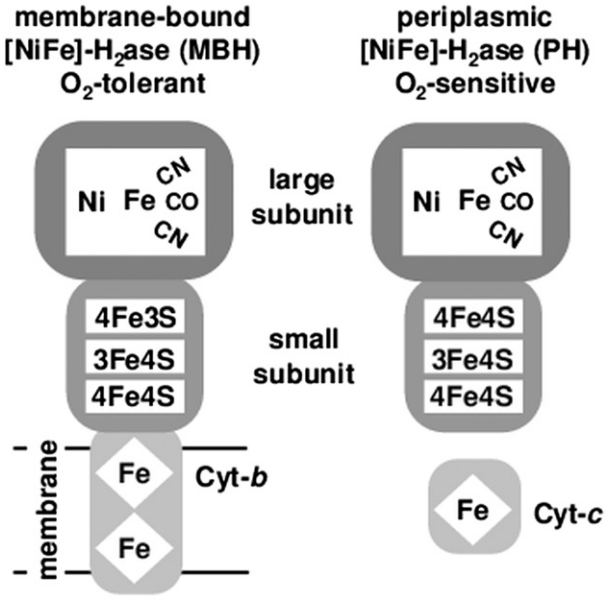

Fig. 1. Schematic organisation of [NiFe]-hydrogenases of the MBH and PH types. Our enzyme preparations lacked the membrane and the cytochrome-*b* or -*c* heme proteins. A proximal [4Fe3S] cluster in the MBHs was identified in crystal structures [14–16,66]. Notably, the *E. coli* hydrogenase II is a membrane associated enzyme not using cyt-*c*, but here grouped among the PHs because of the lack of the two additional cysteines in its small subunit, the presence of which is characteristic for the MBHs.

from *Escherichia coli* (denoted as *Ec*2) is included here as a PH, although it is associated with the cytoplasmic membrane and does not use a *c*-type cytochrome as electron-transfer partner, because it resembles other standard type hydrogenases in terms of its catalytic properties and sensitivity to O_2.

Protein crystallography has revealed the general organisation of the metal cofactors in MBHs [14–16] and PHs [17–20]. In both enzyme types, the [NiFe] site is coordinated by four conserved cysteine residues, two thiolate sulfur atoms of which bridge the Ni and Fe atoms and the other two ligate the nickel, while the iron carries one carbon monoxide (CO) ligand and two cyanide (CN^-) groups [9,21,22]. However, the amino acid sequence accounting for the [NiFe] binding site in the large subunit is not strictly conserved among the various MBH and PH proteins from different organisms [23]. By treatment with various oxidants or reductants, the [NiFe] site can be poised in spectroscopically defined redox states, two of which are associated with reversibly inactivated enzyme, namely the so-called Ni-A and Ni-B states, containing Ni(III) and Fe(II) ions and an oxygen species in the metal-bridging position [24]. This species likely is a hydroxyl (OH^-) in Ni-B whereas for Ni-A the structural assignment is controversial [24,25]. Inactivation of PHs under O_2 or under anoxic conditions and oxidizing potentials favours formation of the Ni-A state, requiring extensive reduction procedures to be reactivated, and Ni-B usually is a minor species [26]. In the MBHs, similar conditions favour Ni-B formation and Ni-A is not observed in most enzymes [9,27,28]. Reactivation of Ni-B under reducing conditions is much faster compared to Ni-A in particular in the MBHs, possibly related to fine-structural differences at the [NiFe] site [29].

The O_2-tolerant MBHs are further distinguished from the PHs by the presence of two additional cysteine residues in the amino acid sequence of the small subunit, located in the vicinity of the binding site for the proximal FeS cluster [11,30,31]. Crystal structures of MBH proteins from *Ralstonia eutropha* [14], *Hydrogenovibrio marinus* [16], and *E. coli* [15] have revealed that these cysteines indeed coordinate three of the four iron atoms of the proximal cluster, transforming it from a cubane [4Fe4S] cluster as in the PHs to a novel [4Fe3S] cluster species. Mutagenesis and spectroscopic studies have shown that the modified proximal cluster is crucial for the O_2-tolerant catalytic behaviour of the MBHs [28,30]. This may be due to the surplus electron donation capacity of the modified cluster to the [NiFe] site, leading to full reduction of metal-bound oxygen species and thereby to rapid reactivation of the enzymes under O_2 [6,7,31]. Vice versa, it may be expected that the not yet crystallized MBHs with the two additional cysteines in their sequence contain a similar [4Fe3S] cluster.

X-ray absorption spectroscopy (XAS) facilitates detection of FeS cluster variations and determination of the nickel coordination at the active site in [NiFe]-H_2ases [29,32–35]. Here, we used XAS to obtain structural parameters of the FeS and [NiFe] cofactors in three O_2-sensitive PHs and four O_2-tolerant MBHs from six organisms. The data suggested similar FeS clusters in the four MBHs, in particular a proximal cluster differing from that in the PHs. The Ni site overall was similar in both enzyme types, but showed increased coordination disorder and weaker nickel–oxygen bonding in the MBHs (Ni-B) compared to the PHs (Ni-A).

2. Materials and methods

2.1. Protein sample preparation

Purified H_2ase proteins, i.e. MBHs from *R. eutropha* HF649 [29], *Aquifex aeolicus* (H_2ase I) [9], *E. coli* (*Ec*1) [36], and *Hydrogenophaga* spec. AH24 [37], and PHs from *Desulfovibrio gigas* [38], *Desulfovibrio fructosovorans* [39], and *E. coli* (*Ec*2) in their oxidized states were prepared following established procedures as described elsewhere [9,28,29,37,39] and concentrated to 0.5–1 mM. The enzymes were purified under microaerobic reducing conditions and poised thereafter mainly in the Ni-B state (MBHs) or Ni-A state (PHs) using air oxidation, as verified by the characteristic and well-known EPR and FTIR spectral signatures (not shown) of the protein preparations [9,22,27–29,36,37,40–42]. This revealed contents ≥65% of the Ni-B state in the MBHs and the Ni-A state in the PHs. Protein solutions (~20 μl) were filled into sample holders for XAS and frozen in liquid nitrogen. Aliquots of the protein samples were used for TXRF to determine the metal contents.

2.2. Metal content quantification

Ni and Fe contents of H_2ase proteins were determined by total-reflection X-ray fluorescence analysis (TXRF) [43] on a PicoFox instrument (Bruker) after adding a gallium elemental standard (Sigma) to the protein solutions (v/v 50:50).

2.3. X-ray absorption spectroscopy

XAS experiments were performed at beamlines KMC-1 of BESSY (Helmholtz Zentrum Berlin, Germany), D2 of HASYLAB (DESY, Hamburg, Germany), 16.5 of SRS (Daresbury, UK), and at the XAS beamline of ANKA (Karlsruhe Institut für Technologie, Karlsruhe, Germany) using standard set-ups (including a double-crystal monochromator) and procedures [44]. Kα fluorescence-detected XAS spectra at the Ni and Fe K-edges were collected for samples held in liquid-helium cryostats at 20 K with energy-resolving multi-element Ge detectors (Canberra or Ortec). XAS spectra were averaged (4–16 scans) after energy calibration of each scan using the spectra of Ni or Fe metal foils as standards, normalized and EXAFS oscillations were extracted as described elsewhere [29,44,45]. The energy scale of XAS spectra was converted to a wavevector (k) scale using E_0 values of 8333 eV (Ni) and 7112 eV (Fe); E_0 was refined to ~7120 eV (Fe) and ~8336 eV (Ni) in the spectral simulations. Unfiltered k^3-weighted EXAFS spectra were used for least-squares curve-fitting simulations with the in-house programme SimX [44] and phase-functions calculated with FEFF8 [46] and Fourier-transform (FT) calculation (S_0^2 values of 0.9 (Ni) and 0.85 (Fe)). The simulation quality was judged by calculation of the filtered R-factor (R_F) [44].

3. Results

3.1. [NiFe]-H_2ase proteins and metal contents

Four O_2-tolerant H_2ases of the MBH type from *R. eutropha* (*Re*), *A. aeolicus* (*Aa*), *E. coli* (H_2ase I, *Ec*1), and *Hydrogenophaga* spec. (*Hs*) and three O_2-sensitive PHs from *E. coli* (H_2ase II, *Ec*2), *D. gigas* (*Dg*), and *D. fructosovorans* (*Df*) were compared. The enzymes were poised mainly in the Ni-B state (MBHs) or Ni-A state (PHs) using air oxidation [9,22,27–29,36,37,40–42]. Iron-to-nickel ratios were determined by TXRF. Within error limits similar values close to 12:1 were observed in the seven proteins (Table 1); the iron atoms belonging to the [NiFe] site and to two four-iron clusters (proximal and distal) and one medial three-iron cluster in the MBHs and PHs. The MBHs mostly showed Fe:Ni ratios at the lower end, presumably reflecting spurious unspecific nickel (<5%) in the samples rather than partial iron loss. These results indicated that the [NiFe] and FeS cofactors in all proteins were intact.

3.2. Fe-XAS on the iron–sulfur clusters

XAS at the Fe K-edge revealed global oxidation states and structural features of the iron sites in the enzymes. The XANES spectra of the MBHs were similar, but differed from those of the PHs by an ~5% larger primary edge maximum and ~0.5 eV higher K-edge energy (~7118.2 eV at 50% level) (Fig. 2A). This indicated overall more oxidized iron in the MBHs [29,33]. Using 12 Fe ions per MBH and a ~3 eV K-edge up-shift for 1 e^- oxidation of sulfur-coordinated mono-iron compounds [47], the presence of an upper limit of about two more Fe(III) ions in the MBHs compared to the PHs was calculated. We note that a steeper K-edge slope due to additional O/N ligands at the proximal FeS cluster [48] may contribute to the energy up-shift in the MBHs and lead to an overestimation of the number of surplus oxidized iron atoms, which therefore may be closer to unity. An ~0.4 eV higher peak energy (~7112.1 eV) of the pre-edge feature was observed in the MBHs. The pre-edge feature is due to transitions of 1*s* electrons into molecular orbitals with mainly Fe*d* character and its energy and shape changes are not straightforwardly related to oxidation state changes of iron in the presence of coordination changes [48].

EXAFS analysis revealed the first-sphere iron coordination and Fe–Fe distances in the H_2ase proteins (Fig. 2B). The Fourier-transforms (FTs) of EXAFS spectra of the MBHs were similar to each other within noise limits, but differed pronouncedly from those of the PHs, in particular regarding the almost two times smaller amplitude of the second FT peak reflecting Fe–Fe distances (Fig. 2B). Notably, the about two-fold lower amplitude of the second FT peak in the MBHs cannot be explained by unspecific iron in the samples, because significant contaminations were not detected in the metal quantification. The first FT peak assigned mainly to iron–sulfur bonds was only slightly diminished in the MBHs, suggesting overall similar iron coordination mostly by thiol groups of cysteines and bridging sulfur atoms in the FeS clusters as in the PHs.

Quantification of the numbers per iron atom of Fe–S and Fe–Fe interactions and of respective interatomic distances by EXAFS simulations, using a two-shell fit approach, revealed an approximately one unit lower coordination number of Fe–Fe distances of ~2.7 Å in the MBHs (N_{Fe-Fe} ~1.6) compared to the PHs (N_{Fe-Fe} ~2.6) as the main result (Table 2A). However, the N_{Fe-Fe} values for the MBHs appeared to be too low to account for the expected three FeS clusters in these enzymes. This result and the lower N_{Fe-S} value suggested interference effects in the EXAFS of the MBHs due to larger Fe–Fe and Fe–S distance spreads, leading to underestimation of the coordination numbers. Accordingly, a more elaborated fit approach included the Fe-ligand bonds of the iron at the active site, two Fe–S shells, and further Fe–Fe distances (Table 2B, Fig. 3). For the PHs, the second fit approach yielded main coordination numbers of Fe–S and Fe–Fe interactions similar to the simple fit approach, only few longer Fe–S bonds, and insignificantly small

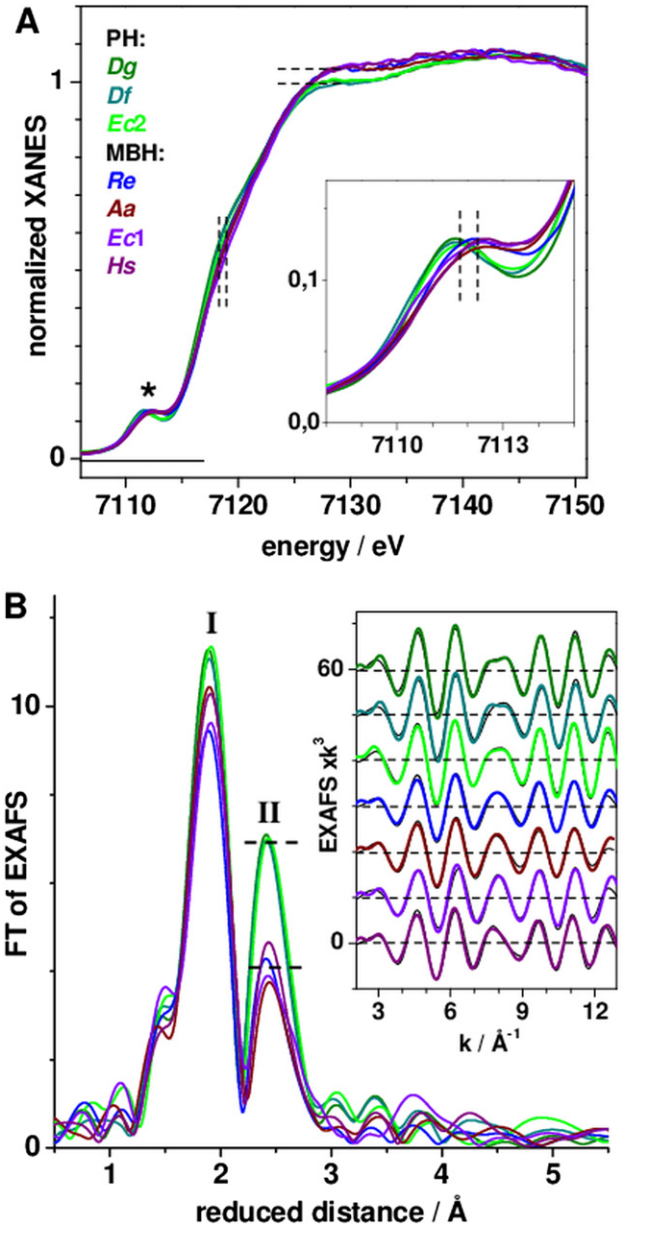

Fig. 2. Fe-XAS spectra of PH and MBH proteins. (A) K-edge absorption spectra and pre-edge features (asterisk) in magnification in the inset. Dashed lines mark spectral changes discussed in the text. (B) Fourier transforms (FTs) of EXAFS spectra of samples as in (A). FTs were calculated for a *k*-range of 2–13 $Å^{-1}$ using $\cos^2$ windows over 10% at both *k*-range ends. Dashes mark the amplitude difference of FT peak II due to Fe–Fe distances. Inset: filtered experimental spectra (Fourier isolation over 1–3.5 Å of reduced distance in the FTs; black lines, vertically displaced for comparison) and simulations (coloured lines, Table 2B).

Table 1
Iron-to-nickel ratios in hydrogenase proteins from TXRF.[a]

H_2ase type	Source organism	Fe/Ni
MBH	*Ralstonia eutropha* (*Re*)	11.3 ± 0.8
	Aquifex aeolicus (*Aa*)	11.8 ± 1.0
	Escherichia coli (*Ec*1)	11.1 ± 1.3
	Hydrogenophaga spec. (*Hs*)	11.7 ± 0.9
	Average MBHs	11.5 ± 0.9
PH	*Desulfovibrio gigas* (*Dg*)	12.4 ± 0.3
	Desulfovibrio fructosovorans (*Df*)	12.6 ± 0.5
	Escherichia coli (*Ec*2)	11.7 ± 0.4
	Average PHs	12.2 ± 0.5

[a] Errors represent standard deviations for measurements on 2–4 independent samples and 2–3 repetitions per sample.

Table 2
Simulation parameters of Fe-EXAFS spectra.[a]

H_2ase type	Source organism	Shell	*N* [per Fe]	*R* [Å]	$2\sigma^2$ [Å^2]	R_F [%]
A						
PH	*Dg*	Fe–S	3.69	2.27	0.007	8.2
		Fe–Fe	2.62	2.71	0.009	
	Df	Fe–S	3.62	2.27	0.007	14.3
		Fe–Fe	2.49	2.71	0.009	
	Ec2	Fe–S	3.79	2.28	0.007	11.9
		Fe–Fe	2.68	2.71	0.009	
MBH	*Re*	Fe–S	3.36	2.28	0.007	11.3
		Fe–Fe	1.62	2.72	0.009	
	Aa	Fe–S	3.28	2.28	0.007	14.7
		Fe–Fe	1.42	2.72	0.009	
	*Ec*1	Fe–S	3.45	2.28	0.007	19.5
		Fe–Fe	1.33	2.72	0.009	
	Hs	Fe–S	3.32	2.29	0.007	14.1
		Fe–Fe	1.54	2.72	0.009	
B						
PH	*Dg*	Fe–C/N/O	0.39	2.03	0.002	6.2
		Fe–S	3.61	2.29	0.007	
		Fe–S	0.39	2.56	0.007	
		Fe–Fe	2.26	2.72	0.008	
		Fe–Fe	0.22	2.96	0.008	
		Fe–Fe	0.06	3.16	0.008	
	Df	Fe–C/N/O	0.42	2.01	0.002	9.7
		Fe–S	3.53	2.29	0.007	
		Fe–S	0.57	2.58	0.007	
		Fe–Fe	2.25	2.71	0.008	
		Fe–Fe	0.28	2.94	0.008	
		Fe–Fe	0.07	3.23	0.008	
	Ec2	Fe–C/N/O	0.46	2.02	0.002	8.3
		Fe–S	3.84	2.29	0.007	
		Fe–S	0.16	2.56	0.007	
		Fe–Fe	2.39	2.72	0.008	
		Fe–Fe	0.17	2.90	0.008	
		Fe–Fe	0.07	3.20	0.008	
MBH	*Re*	Fe–C/N/O	0.39	1.99	0.002	5.7
		Fe–S	3.21	2.29	0.007	
		Fe–S	0.79	2.61	0.007	
		Fe–Fe	1.33	2.68	0.008	
		Fe–Fe	0.68	2.79	0.008	
		Fe–Fe	0.39	3.41	0.008	
	Aa	Fe–C/N/O	0.29	2.04	0.002	11.6
		Fe–S	2.97	2.28	0.007	
		Fe–S	0.98	2.63	0.007	
		Fe–Fe	1.14	2.65	0.008	
		Fe–Fe	1.11	2.76	0.008	
		Fe–Fe	0.28	3.45	0.008	
	*Ec*1	Fe–C/N/O	0.53	2.06	0.002	13.6
		Fe–S	3.22	2.29	0.007	
		Fe–S	0.77	2.59	0.007	
		Fe–Fe	1.27	2.67	0.008	
		Fe–Fe	0.95	2.79	0.008	
		Fe–Fe	0.36	3.42	0.008	
	Hs	Fe–C/N/O	0.55	2.02	0.002	8.4
		Fe–S	3.06	2.31	0.007	
		Fe–S	0.93	2.60	0.007	
		Fe–Fe	1.02	2.69	0.008	
		Fe–Fe	0.86	2.77	0.008	
		Fe–Fe	0.55	3.38	0.008	

[a] *N*, coordination number; *R*, interatomic distance; $2\sigma^2$, Debye–Waller factor. (A) 2-shell fit approach; $2\sigma^2$ values were determined from the *Dg* PH spectrum and fixed in the fits of the other spectra. (B) 6-shell approach; $2\sigma^2$ values were derived as in (A), the sum of the N_{Fe-S} values was restraint to 4, the sum of the N_{Fe-Fe} values was restraint to ≤2.6. R_F [44] was calculated for reduced distances of 1–3 Å in (A) and 1–3.5 Å in (B).

contributions from longer Fe–Fe distances (Fig. 3). For both PHs and MBHs, the small $N_{Fe-C/N/O}$ values were similar and in agreement with 2 Fe–CN$^-$, 1 Fe–CO, and 1 Fe–O bonds at the active site iron (and the Fe–$N_{histidine}$ bond at the distal FeS cluster in the PHs). The main differences in the structural parameters of the MBHs (Fig. 3) were a larger number of long Fe–S bonds (~2.6 Å), two discernable shorter Fe–Fe distances (~2.65 Å, ~2.8 Å), and an additional longer Fe–Fe distance (~3.4 Å). Taking the Debye–Waller parameter (σ) of ~0.06 Å of the

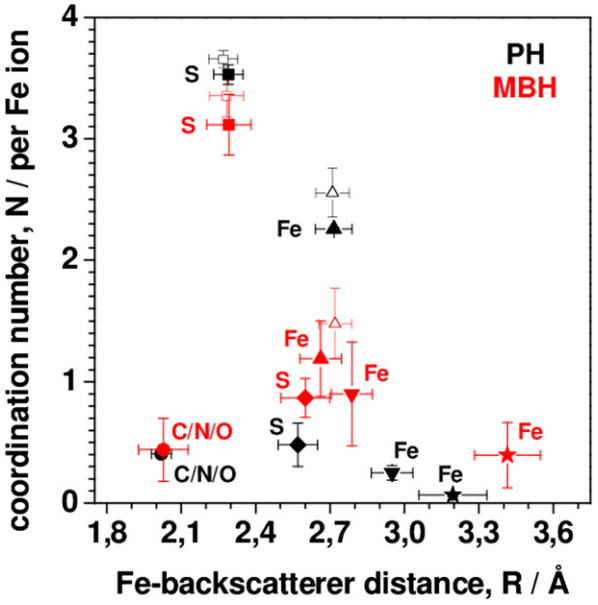

Fig. 3. Simulation results of Fe-EXAFS spectra. Mean values for PHs (black) and MBHs (red) of data in Table 2A (open symbols) and 2B (solid symbols) are shown. Error bars denote: x-error, largest minus smallest fitted *R*-value plus Debye–Waller factor (σ); y-error, largest minus smallest fitted *N*-value. Backscatterer species (Fe–C/N/O, –S, –Fe) are indicated.

Fe–Fe distance distribution into account (Table 2B), shortest and longest Fe–Fe distances of ~2.60 Å and ~2.85 Å, besides those of ~2.7 Å, were suggested in the MBHs, which were barely detectable in the PHs.

For the PHs, a total number of ~2.7 Å Fe–Fe/Ni interactions of 31 was calculated for the [NiFe] site and the two [4Fe4S] and one [3Fe4S] clusters, translating into an $N_{Fe-Fe/Ni}$ value of 2.58 per Fe ion, in agreement with the experimental value (~2.6). From the mean $N_{Fe-Fe/Ni}$ values in the MBHs of ~2 (shorter distances) and ~0.4 (longer distance) and the 12 Fe ions, total numbers of Fe–Fe/Ni interactions of ~24 and 4–5 resulted, amounting to ~12 shorter 2.60–2.85 Å Fe–Fe distances and 2–3 longer distances of ~3.4 Å (and one Fe–Ni distance). The MBHs contain similar medial [3Fe4S] and distal [4Fe4S] clusters as the PHs with expected 9 Fe–Fe distances of ~2.7 Å [14–16]. Accordingly, the proximal FeS cluster in the MBHs was characterized by ~3 shorter and ~2 longer Fe–Fe distances unlike typical [4Fe4S] clusters, but compatible with a structure showing a three-iron unit and a more isolated iron atom at ~3.4 Å to two of the other irons. Notably, Fe–Fe distances longer than ~4 Å for small coordination numbers are difficult to detect by EXAFS and hence were not analyzed. In the crystal structures of oxidized *Ec*1 and *H. marinus* MBHs, quite similar Fe–Fe distance distributions were observed for the proximal [4Fe3S] cluster, including mostly 3 distances of about 2.6–2.9 Å, 2 distances of about 3.0–3.6 Å, and a long distance of roughly 4–5 Å [15,16].

3.3. Ni-XAS on the active site structure

XAS at the Ni K-edge was used to determine the coordination of the active site nickel. The XANES spectra of the PHs and MBHs overall were rather similar and indicative of predominantly sulfur-coordinated nickel [29,34]. The low primary edge maxima suggested a square-pyramidal coordination geometry at the nickel. The spectra of the MBHs differed from those of the PHs by a slightly larger first edge maximum (~8350 eV) and a smaller secondary maximum (~8365 eV) (Fig. 4A). The first edge maximum of XANES spectra from [NiFe]-H_2ases is increased by terminal oxygen ligands at the nickel and the secondary maximum by shorter Ni–O bonds from Ni–Fe bridging oxygen species [29,34,49]. The edge shape of the MBHs thus suggested more terminal binding of the oxygen species at the nickel, as identified by the EXAFS analysis below.

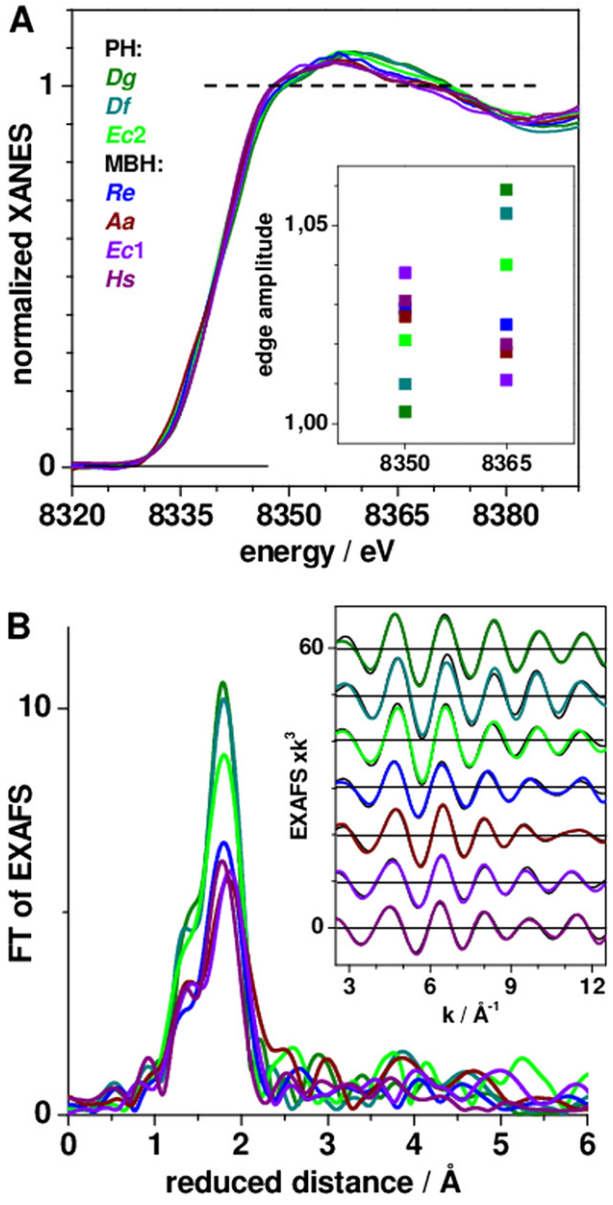

Fig. 4. Ni-XAS spectra of PH and MBH proteins. (A) K-edge spectra of enzymes mostly in the Ni-A (PHs) or Ni-B (MBHs) states (dashes mark the unity level) and edge amplitudes at two energies in the inset. (B) Fourier-transforms (FTs) of EXAFS spectra of samples as in (A). FTs were calculated for a *k*-range of 2–12.5 $Å^{-1}$ using $\cos^2$ windows as specified in Fig. 2. Inset: filtered experimental spectra (Fourier isolation over 1–2.5 Å of reduced distance in the FTs; black lines, vertically displaced) and simulations (coloured lines, Table 3).

Ni-EXAFS spectra of the H_2ase proteins are shown in Fig. 4B. Visual inspection revealed significantly diminished amplitudes of the main FT peak in the spectra of the MBHs compared to the PHs. However, the EXAFS simulation results were in agreement with globally similar first-sphere coordination of the nickel in the PHs and MBHs by four sulfur atoms (from the four conserved cysteines) and one oxygen ligand (Table 3). The short Ni–O bonds of ~1.85 Å in the PHs were in agreement with crystal structures of PHs in the Ni-A state [18,19,50,51]. Subtle structural differences in the MBHs compared to the PHs were detectable, namely by ~0.05 Å longer Ni–O and main Ni–S bonds, an ~2-times larger Debye–Waller parameter ($2\sigma^2$) of the shorter Ni–S bonds, and an ~0.1 Å shorter mean Ni–Fe distance (Table 3). The $2\sigma^2$ values of the shorter Ni–S distances suggested a greater spread of bond lengths of ±0.08 Å compared to ±0.05 Å in the PHs, reflecting a more disordered Ni coordination in the MBHs. Notably, inclusion of a second and longer Ni–O distance (i.e. >2.2 Å) in the EXAFS simulations was possible

Table 3
Simulation parameters of Ni-EXAFS spectra.[a]

H_2ase type	Source organism	Shell	*N* [per Ni]	*R* [Å]	$2\sigma^2$ [$Å^2$]	R_F [%]
PH	*Dg*	Ni–O	0.82	1.85	0.004[b]	11.2
		Ni–S	2.73	2.18	0.005	
		Ni–S	1.27	2.71	0.004[b]	
		Ni–Fe	1[b]	2.75	0.005[b]	
	Df	Ni–O	0.94	1.84	0.004[b]	15.4
		Ni–S	2.70	2.18	0.006	
		Ni–S	1.30	2.68	0.004[b]	
		Ni–Fe	1[b]	2.72	0.005[b]	
	Ec2	Ni–O	1.02	1.86	0.004[b]	13.4
		Ni–S	2.66	2.19	0.008	
		Ni–S	1.34	2.64	0.004[b]	
		Ni–Fe	1[b]	2.69	0.005[b]	
MBH	*Re*	Ni–O	0.67	1.88	0.004[b]	12.1
		Ni–S	2.71	2.20	0.013	
		Ni–S	1.29	2.62	0.004[b]	
		Ni–Fe	1[b]	2.64	0.005[b]	
	Aa	Ni–O	0.79	1.87	0.004[b]	9.4
		Ni–S	2.74	2.21	0.014	
		Ni–S	1.26	2.63	0.004[b]	
		Ni–Fe	1[b]	2.67	0.005[b]	
	Ec1	Ni–O	0.75	1.90	0.004[b]	12.8
		Ni–S	2.55	2.23	0.012	
		Ni–S	1.45	2.60	0.004[b]	
		Ni–Fe	1[b]	2.62	0.005[b]	
	Hs	Ni–O	0.69	1.87	0.004[b]	10.1
		Ni–S	2.65	2.22	0.011	
		Ni–S	1.35	2.59	0.004[b]	
		Ni–Fe	1[b]	2.60	0.005[b]	

The sum of the N_{Ni-S} values was restraint to 4. R_F [44] was calculated for reduced distances of 1–2.5 Å.
[a] *N*, coordination number; *R*, Ni-backscatterer distance; $2\sigma^2$, Debye–Waller factor.
[b] Parameters that were fixed to physically reasonable values in the fit procedure.

in all cases (not shown). However, we consider respective simulation results as insignificant because inclusion of a longer Ni–O distance did not improve the fit quality and long Ni–O distances cannot be reliably discriminated from the shorter Ni–S distances due to considerable spectral overlap. Also the XANES data suggested only one oxygen ligand in the first coordination sphere of nickel.

Crystal structures for PHs in the Ni-A and Ni-B states and for oxidized MBHs (Ni-B) are available [15–19,39,50–52] and XAS data were obtained in this work for oxidized MBHs (Ni-B) and PHs (Ni-A) and were reported previously for PHs in the Ni-B state [32,53]. The mean Fe–S distances from crystallography and XAS and for Ni-A and Ni-B were very similar for MBHs and PHs, showing that both methods provide essentially comparable results (Table 4). The Ni–O bonds for PHs in Ni-B were ~0.06 Å shorter than in Ni-A whereas for MBHs in Ni-B they were even slightly longer than for PHs in Ni-A. The Ni–Fe distance for PHs in Ni-A was longer than for PHs in Ni-B and shortest for MBHs in Ni-B. These observations and our XANES data suggested a more terminal position at the nickel of oxygen species in the Ni–Fe bridging position in MBHs in the Ni-B state compared to PHs in the Ni-A and Ni-B states.

4. Discussion

Our Fe-XAS analysis consistently revealed an overall different structure of FeS clusters in the four MBHs compared to the three PHs in their oxidized states. Recent crystal structures have shown that instead of a conventional [4Fe4S] cubane cluster as in the PHs, the MBHs bind a novel [4Fe3S] cluster in the proximal position [14–16], comprising a three-iron unit and a more separated iron atom (Fig. 5A). The modified structure is facilitated by ligation of the [4Fe3S] cluster to two additional cysteine residues, present in the amino acid sequence of the small subunit of virtually all O_2-tolerant MBHs, but missing in the PHs. The [4Fe3S] cluster in the MBHs can undergo two oxidative transitions in a

Table 4
Interatomic distances in the [NiFe] cofactor from XAS and crystallography.

	MBH	PH	
	Oxidized (Ni-B)	Ni-B	Ni-A
	Distance [Å] XAS, crystallography, average		
Ni–μO	1.88(1), 1.83(6)[a], 1.86(5)	1.87(4)[b], 1.73(11)[c], 1.77(11)	1.85(1), 1.85(9)[d], 1.85(7)
Ni–S	2.35(2), 2.34(4)[a], 2.34(3)	2.33(3)[b], 2.35(6)[c], 2.34(5)	2.34(1), 2.36(5)[d], 2.35(4)
Ni–Fe	2.63(3), 2.86(3)[a], 2.75(13)	2.79(10)[b], 2.77(11)[c], 2.77(10)	2.72(3), 2.87(8)[d], 2.82(10)

[a] Mean values from MBH crystal structures (PDB ID: 3AYY and PDB ID: 3AYZ of *Ec*1 and PDB ID: 3USC and PDB ID: 3USE of *Hydrogenovibrio marinus*).
[b] Mean values from XAS data for PHs from *Desulfovibrio desulfuricans* and *Allochromatium vinosum* [32,53].
[c] Mean values from PH crystal structures 1WUJ, 1YRQ, 2FRV, 1WUK.
[d] 1WUI, 1YQW, 1YQ9, 3MYR, 3CUR, 1WUH of *D. vulgaris* Miyazaki F, *Df*, *Dg*, and *A. vinosum*; standard deviations in parenthesis.

narrow potential range, instead of only one as the [4Fe4S] cluster in the PHs [13,27,28,54]. We have detected more oxidized iron in the MBHs compared to the PHs, in agreement with a higher oxidation state of the proximal cluster in the MBH preparations. The Fe–Fe distances and coordination numbers from XAS are well in agreement with crystal data for oxidized PHs and MBHs. Accordingly, the particularly long Fe–Fe distances could be assigned to those Fe ions of the proximal cluster, which are ligated by the additional cysteines in the MBHs (Fig. 5A). In addition, the lower coordination number of ~2.7 Å Fe–Fe distances is diagnostic for the altered proximal cluster in the MBHs. We thus confirmed the modified structure of the proximal cluster in the *Re* and *Ec*1 MBHs, for which crystal data is available [14,15], and for those MBHs, which have not been crystallized yet, but studied by other spectroscopic methods [9,13,37,54,55].

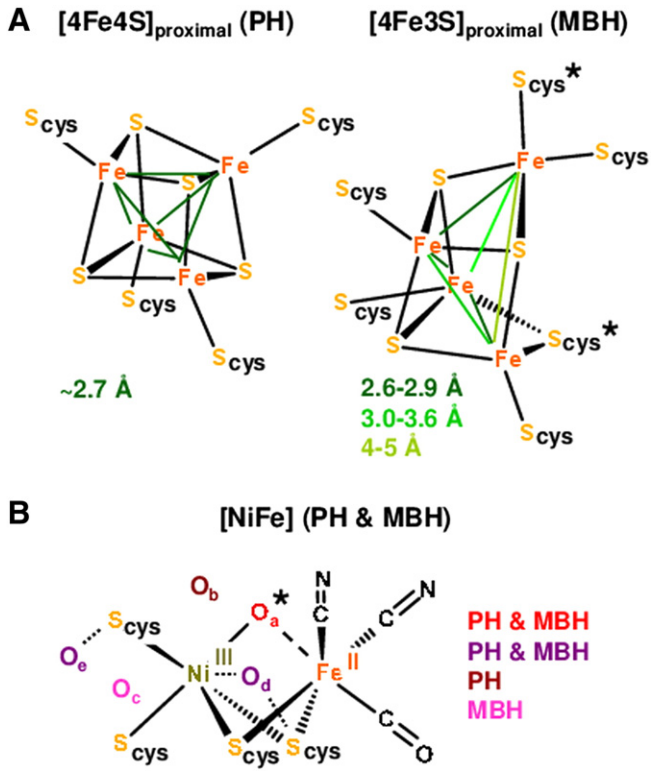

Fig. 5. Structural models of metal centres in PH and MBH proteins. (A) Proximal FeS clusters in crystal structures (see Table 4). Approximate Fe–Fe distances from crystallography and XAS are indicated. Asterisks mark the two additional cysteine (cys) residues in the small subunit of the MBHs. (B) Model for oxidized [NiFe] cofactors with oxygen (O) sites detected by crystallography and XAS in the Ni-A and Ni-B states (O_a, asterisk) or assigned in crystal structures of oxidized PH or MBH proteins (O_{b-e}). See Table 4 and the text for further details.

The Ni-XAS analysis revealed a similar coordination of the nickel atom by four sulfurs, most likely belonging to the thiol groups of the cysteine residues conserved in the large subunit of all [NiFe]-H_2ases and observed in the crystallographic data of PHs and MBHs. The global configuration of the oxidized [NiFe] cofactor thus is comparable in all studied enzymes (Fig. 5B). In addition, about one short Ni–O bond was detected by XAS both in the PHs and MBHs. The short Ni–O bond lengths suggest that the oxygen species is located in the Ni–Fe bridging position. Both the XANES and EXAFS analyses provided no evidence for further oxygen species directly bound to the nickel in all enzymes. If there were further oxygen species, they would be located in the second coordination sphere of nickel so that their long Ni–O distances could not be discriminated by XAS from the Ni–S distances.

Differences in the EXAFS structural parameters of the [NiFe] site in the MBHs (Ni-B) compared to the PHs (Ni-A) included a larger Ni–S bond lengths spread, a shorter Ni–Fe distance, and a longer Ni–O bond in the MBHs. In contrast, the available data seem to suggest that in PHs the bond to the nickel of the Ni–Fe bridging oxygen species in Ni-B is shorter than in Ni-A. Furthermore, the EPR g-values and the Fe–CO/CN^- vibrational frequencies from FTIR differ considerably between Ni-A and Ni-B in PHs [4,24], but mostly less for Ni-B in MBHs and PHs [9,27,30,56]. These results imply significant structural differences at the [NiFe] site of the MBHs in Ni-B and the PHs in Ni-A and more similar Ni-B structures in MBHs and PHs. A weaker Ni–O bond in the MBHs in Ni-B is conceivable (Fig. 5B), which could be related to the faster activation of the Ni-B state in MBHs compared to PHs.

The location of oxygen species around the [NiFe] cofactor in Ni-A or Ni-B based on crystal structures is controversial (Fig. 5B). In oxidized PHs and MBHs, a Ni–Fe bridging O-atom (O_a) consistently was observed and further O-species were assigned at various locations (Fig. 5B). An oxygen (O_b) close to O_a was found only in various PHs, but not in MBHs. This has been interpreted as a (hydro)peroxo (OOH^-) bridge in the Ni-A state [18,50,57], which might result from the two-electron reduction of O_2. Notably, the crystal structure of oxidized *Allochromatium vinosum* PH did not show a second O-species close to the Ni [19]. The Ni-B state presumably contains a Ni–Fe bridging hydroxo (OH^-) ligand both in PHs and MBHs [6,24]. In the MBHs, the Ni-B state has been proposed to be favoured over Ni-A by the surplus electron donation capacity of the proximal [4Fe3S] cluster, facilitating four-electron reduction of O_2 at the [NiFe] site to the bridging OH^- and, i.e., a water molecule [7,31,54]. However, Ni-A and Ni-B formation also under anoxic conditions in PHs and MBHs [9,22,29,58] and ^{17}O labelling experiments on PHs [59,60] suggested that the bridging O-ligand in Ni-A and Ni-B could stem from water as well. A possible mechanism, which accounts for these results, would be oxidation of Ni(II) in reduced enzymes to Ni(III) directly by O_2 (aerobic) or via the FeS clusters by external oxidants (anoxic), causing bridging OH^- binding and localization of reduced oxygen species, for example water molecules from O_2 reduction or from the surrounding, at secondary sites around the [NiFe] cofactor.

Two further oxygen sites have been assigned in crystal structures, which presumably are due to oxidation of Ni–Fe bridging (O_d) or

terminal (O_e) thiol ligands to sulfenate (cysSO) groups in irreversibly inactivated [NiFe] cofactors [29,58] (Fig. 5B). In the *Re* MBH, a bridging sulfenate manifests in a long (~3.1 Å) Ni–Fe distance and altered XANES spectrum due to coordination of its O-atom at the nickel [29]. That such features were not prominent in our MBH and PH preparations suggests low contents of bridging sulfenates. Terminal sulfenates are not excluded because their long Ni–O distances were not resolved here. In any event, the available spectroscopy and crystallography data seem to suggest that species showing occupation of the O_d and O_e sites are unrelated to the specific characteristics of the Ni-A and Ni-B states. Rather, such species may correspond to EPR-silent states in oxidized PH [41,61] of MBH preparations [9,22] as observed by FTIR spectroscopy.

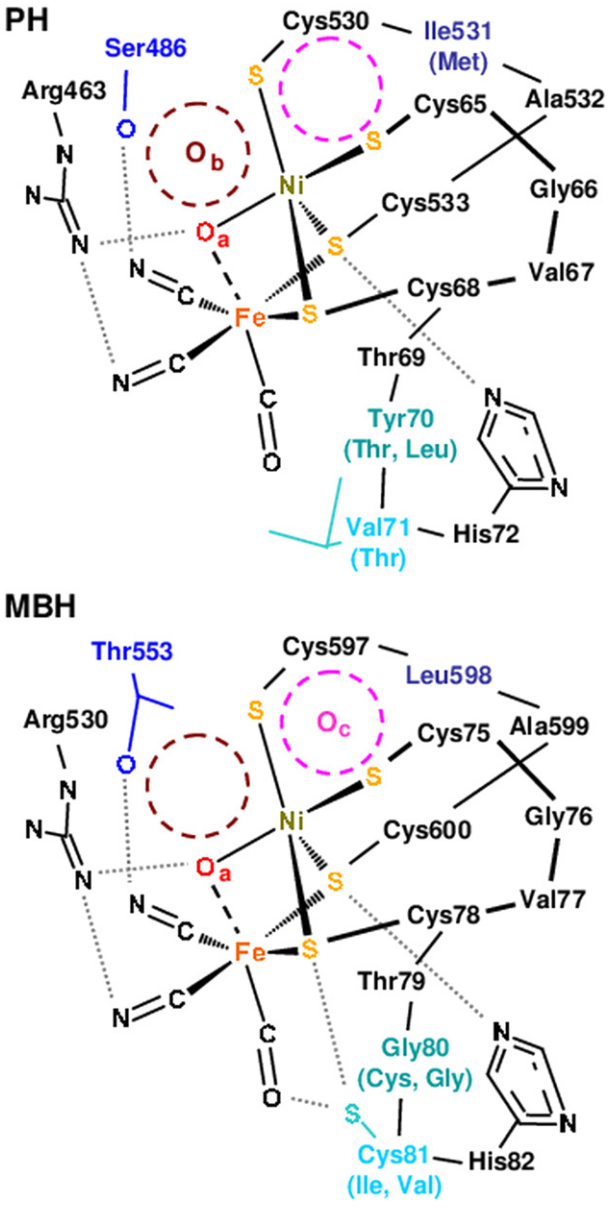

Fig. 6. Amino acid exchanges around the [NiFe] cofactor in PHs and MBHs. Schemes use *D. gigas* PH (top) or *R. eutropha* MBH (bottom) numbering and were based on crystal structures (see Table 4) and sequence data, bond lengths were not drawn to scale. Val71 in the *Dg* and *Df* PHs is Thr in the *Ec*2 and *D. vulgaris* Miyazaki-F PHs, Val in the *Ec*1 MBH, Cys in the *Re* and *Hydrogenovibrio marinus* (*Hm*) MBHs, and Ile in the *Aa* MBH. Tyr70 in the *Desulfovibrio* PHs is Thr in the *Ec*2 PH, Leu in the *Allochromatium vinosum* and *Thiocapsa roseopersicina* PHs, Gly in the *Re*, *Ec*1, and *Hm* MBHs, and Cys in the *Aa* MBH. Ser486 in PHs is Thr in MBHs. Ile531 in PHs (Met in the *Ec*2 PH) is Leu in MBHs. Dashed circles mark oxygen sites (Fig. 5) assigned in structures only of PHs (O_b) [18,50,57] or MBHs (O_c) [15,16]. Dotted lines denote potential hydrogen bonding interactions.

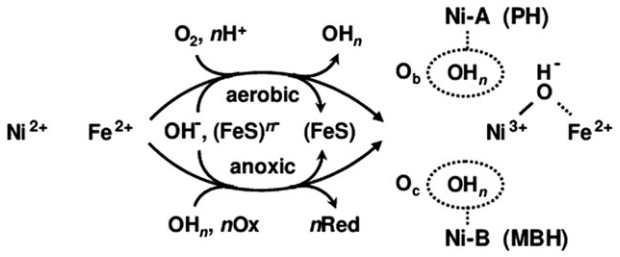

Fig. 7. Hypothesis on oxidative [NiFe] cofactor inactivation in MBHs and PHs. Starting with reduced enzymes, Ni(II) oxidation to Ni(III) directly by O_2 (aerobic) or indirectly by exogenous oxidants (anoxic) causes Ni–Fe bridging OH^- binding in Ni-A and Ni-B. Further oxygen-species reduction (aerobic) or further electron abstraction (anoxic) leads to oxidation of the FeS clusters. Similar reduced oxygen species, for example water molecules from O_2 reduction (aerobic) or from the environment (anoxic), are then localized at the O_b site in the Ni-A state of O_2-sensitive PHs or at the O_c site in the Ni-B state of O_2-tolerant MBHs (compare Fig. 6) and presumably at further less specific positions in the proteins.

Remarkably, in crystal structures of oxidized MBHs further secondary oxygen sites (O_c) have been assigned [15,16], which were not observed in PH structures (Fig. 5B). Vice versa, O_b site occupation was only observed in Ni-A structures of PHs. It is thus tempting to speculate that binding of reduced oxygen species occurs at the O_b site in the Ni-A state of the PHs, but at the O_c site in the Ni-B state of the MBHs. Also for the Ni-B state of the PHs, O_c site occupation is an option. Disfavouring of the O_b site also may explain that the MBHs in contrast to the PHs are not inhibited by carbon monoxide [55,62], which binds at the nickel roughly at the O_b site in the PHs [63]. Oxygen species binding at the O_c site instead of the O_b site therefore could be a discriminator between the Ni-B and Ni-A states. According to our XAS data, respective oxygen species presumably are not directly coordinated to the nickel.

Structural variations around the [NiFe] cofactor may explain why Ni-B is favoured over Ni-A in the MBHs. Four residues close to the active site, Ser486, Ile531, Tyr70, and Val71 (numbering of the *Dg* PH), are not conserved between PHs and MBHs (Fig. 6). Val71 and Tyr70 found in many PHs are remote from the O_a and O_c sites and one of these residues is replaced by a cysteine in most MBHs (Fig. 6). Ser486 in the PHs is close to the O_b site and changed to Thr in all MBHs whereas Ile531 in most PHs is close to the Qc site and changed to Leu in all MBHs. The amino acid variations in the MBHs may affect, for example, hydrogen bonding of the metal ligating groups, thereby favouring oxygen species at the O_c site and destabilization of the Ni–Fe bridging OH^- (Fig. 6). Presumably, it is the concerted effect of the amino acid exchanges that favours the Ni-B state of the [NiFe] cofactor in oxidized MBHs.

In conclusion, the modified structure and redox behaviour of the proximal [4Fe3S] cluster, in combination with more subtle structural alterations at the [NiFe] cofactor including different localizations of oxygen species in the rapidly reactivated Ni-B state, are important determinants of the O_2-tolerant hydrogen chemistry in the MBHs (Fig. 7). Their in vivo activity thus is expected to depend on the relative concentrations of H_2, O_2, and protons, as well as on the ambient potential controlling the redox states of the FeS clusters and of the exogenous electron transfer partners. Deeper insights into the complex interplay between these parameters in the MBHs and in the other types of O_2-tolerant [NiFe]-H_2ases [7,64,65] may lead to a generalized understanding of hydrogen catalysis in the presence of oxygen.

Acknowledgements

M.H. thanks the Deutsche Forschungsgemeinschaft (DFG) for a Heisenberg Fellowship and the DFG (grants Ha3265/3-1 and Ha3265/6-1) and the Bundesministerium für Bildung und Wissenschaft (grant 05K14KE1 within the Röntgen-Angström Cluster) for the financial support. A.L.D.L thanks MINECO (project CTQ2012-32448) for the

financial support. F.A.A. is a Royal Society Wolfson Research Merit Award holder. We thank the beamline scientists F. Schäfers (BESSY at HZB, Berlin), W. Meyer-Klaucke (EMBL at DESY, Hamburg), B. Bilsborough (SRS at Daresbury, UK), and S. Mangold (ANKA at KIT, Karlsruhe) for the technical assistance and H. Dau (FU-Berlin) for providing access to XAS equipment at BESSY. We thank J. Fritsch (Humboldt Universität zu Berlin) for the preparation of the *Re* MBH samples and P. Infossi and M.-T. Giudici-Orticoni (CNRS Marseille) for generously providing the *A. aeolicus* protein.

References

[1] R. Cammack, M. Frey, R. Robson (Eds.), Hydrogen as a Fuel: Learning from Nature, Taylor & Francis, London, UK, 1997.
[2] Special issue on hydrogenases, Chem. Rev. 107 (2007).
[3] P.M. Vignais, B. Billoud, Occurrence, classification, and biological function of hydrogenases: an overview, Chem. Rev. 107 (2007) 4206–4272.
[4] A.L. De Lacey, V.M. Fernandez, M. Rousset, R. Cammack, Activation and inactivation of hydrogenase function and the catalytic cycle: spectroelectrochemical studies, Chem. Rev. 107 (2007) 4304–4330.
[5] K.A. Vincent, A. Parkin, O. Lenz, S.P. Albracht, J.C. Fontecilla-Camps, R. Cammack, B. Friedrich, F.A. Armstrong, Electrochemical definitions of O_2 sensitivity and oxidative inactivation in hydrogenases, J. Am. Chem. Soc. 127 (2005) 18179–18189.
[6] H.S. Shafaat, O. Rüdiger, H. Ogata, W. Lubitz, [NiFe] hydrogenases: a common active site for hydrogen metabolism under diverse conditions, Biochim. Biophys. Acta 1827 (2013) 986–1002.
[7] J. Fritsch, O. Lenz, B. Friedrich, Structure, function and biosynthesis of O_2-tolerant hydrogenases, Nat. Rev. Microbiol. 11 (2013) 106–114.
[8] A. Parkin, F. Sargent, The hows and whys of aerobic H_2 metabolism, Curr. Opin. Chem. Biol. 16 (2012) 26–34.
[9] M.E. Pandelia, V. Fourmond, P. Tron-Infossi, E. Lojou, P. Bertrand, C. Legèr, M.T. Giudici-Orticoni, W. Lubitz, Membrane-bound hydrogenase I from the hyperthermophilic bacterium *Aquifex aeolicus*: enzyme activation, redox intermediates and oxygen tolerance, J. Am. Chem. Soc. 132 (2010) 6991–7004.
[10] S.P. Albracht, Nickel hydrogenases: in search of the active site, Biochim. Biophys. Acta 1188 (1994) 167–204.
[11] M.E. Pandelia, W. Lubitz, W. Nitschke, Evolution and diversification of Group 1 [NiFe] hydrogenases. Is there a phylogenetic marker for O_2-tolerance? Biochim. Biophys. Acta 1817 (2012) 1565–1575.
[12] C. Schäfer, B. Friedrich, O. Lenz, C. Schäfer, B. Friedrich, O. Lenz, Novel, oxygen-insensitive group 5 [NiFe]-hydrogenase in Ralstonia eutropha, Appl. Environ. Microbiol. 79 (2014) 5137–5145.
[13] W. Lubitz, H. Ogata, O. Rüdiger, E. Reijerse, Hydrogenases, Chem. Rev. 114 (2014) 4081–4148.
[14] J. Fritsch, P. Scheerer, S. Frielingsdorf, S. Kroschinsky, B. Friedrich, O. Lenz, C.M. Spahn, The crystal structure of an oxygen-tolerant hydrogenase uncovers a novel iron–sulphur centre, Nature 479 (2011) 249–252.
[15] A. Volbeda, P. Amara, C. Darnault, J.M. Mouesca, A. Parkin, M.M. Roessler, F.A. Armstrong, J.C. Fontecilla-Camps, X-ray crystallographic and computational studies of the O_2-tolerant [NiFe]-hydrogenase 1 from *Escherichia coli*, Proc. Natl. Acad. Sci. U. S. A. 109 (2012) 5305–5310.
[16] Y. Shomura, K.S. Yoon, H. Nishihara, Y. Higuchi, Structural basis for a [4Fe–3S] cluster in the oxygen-tolerant membrane-bound [NiFe]-hydrogenase, Nature 479 (2011) 253–256.
[17] A. Volbeda, M.H. Charon, C. Piras, E.C. Hatchikian, M. Frey, J.C. Fontecilla-Camps, Crystal structure of the nickel–iron hydrogenase from *Desulfovibrio gigas*, Nature 373 (1995) 580–587.
[18] A. Volbeda, L. Martin, C. Cavazza, M. Matho, B.W. Faber, W. Roseboom, S.P. Albracht, E. Garcin, M. Rousset, J.C. Fontecilla-Camps, Structural differences between the ready and unready oxidized states of [NiFe] hydrogenases, J. Biol. Inorg. Chem. 10 (2005) 239–249.
[19] H. Ogata, P. Kellers, W. Lubitz, The crystal structure of the [NiFe] hydrogenase from the photosynthetic bacterium *Allochromatium vinosum*: characterization of the oxidized enzyme (Ni-A state), J. Mol. Biol. 402 (2010) 428–444.
[20] Y. Higuchi, H. Ogata, K. Miki, N. Yasuoka, T. Yagi, Removal of the bridging ligand atom in the Ni–Fe active site of [NiFe] hydrogenase upon reduction with H_2, as revealed by X-ray structure analysis at 1.4 A resolution, Structure 7 (1999) 549–557.
[21] A.J. Pierik, W. Roseboom, R.P. Happe, K.A. Bagley, S.P. Albracht, Carbon monoxide and cyanide as intrinsic ligands to iron in the active site of [NiFe]-hydrogenases. NiFe(CN)2CO, biology's way to activate H_2, J. Biol. Chem. 274 (1999) 3331–3337.
[22] M. Saggu, I. Zebger, M. Ludwig, O. Lenz, B. Friedrich, P. Hildebrandt, F. Lendzian, Spectroscopic insights into the oxygen-tolerant membrane-associated [NiFe] hydrogenase of *Ralstonia eutropha* H16, J. Biol. Chem. 284 (2009) 16264–16276.
[23] O. Lenz, M. Ludwig, T. Schubert, I. Burstel, S. Ganskow, T. Goris, A. Schwarze, B. Friedrich, H_2 conversion in the presence of O_2 as performed by the membrane-bound [NiFe]-hydrogenase of *Ralstonia eutropha*, ChemPhysChem 11 (2010) 1107–1119.
[24] W. Lubitz, E. Reijerse, M. van Gastel, [NiFe] and [FeFe] hydrogenases studied by advanced magnetic resonance techniques, Chem. Rev. 107 (2007) 4331–4365.
[25] M.E. Pandelia, H. Ogata, W. Lubitz, Intermediates in the catalytic cycle of [NiFe] hydrogenase: functional spectroscopy of the active site, ChemPhysChem 11 (2010) 1127–1140.
[26] F.A. Armstrong, Hydrogenases: active site puzzles and progress, Curr. Opin. Chem. Biol. 8 (2004) 133–140.
[27] M. Saggu, C. Teutloff, M. Ludwig, M. Brecht, M.E. Pandelia, O. Lenz, B. Friedrich, W. Lubitz, P. Hildebrandt, F. Lendzian, R. Bittl, Comparison of the membrane-bound [NiFe] hydrogenases from *R. eutropha* H16 and *D. vulgaris* Miyazaki F in the oxidized ready state by pulsed EPR, Phys. Chem. Chem. Phys. 12 (2010) 2139–2148.
[28] M.M. Roessler, R.M. Evans, R.A. Davies, J. Harmer, F.A. Armstrong, EPR spectroscopic studies of the Fe–S clusters in the O2-tolerant [NiFe]-hydrogenase Hyd-1 from *Escherichia coli* and characterization of the unique [4Fe–3S] cluster by HYSCORE, J. Am. Chem. Soc. 134 (2012) 15581–15594.
[29] J. Fritsch, S. Löscher, O. Sanganas, E. Siebert, I. Zebger, M. Stein, M. Ludwig, A.L. De Lacey, H. Dau, B. Friedrich, O. Lenz, M. Haumann, [NiFe]- and [FeS]-cofactors in the membrane-bound hydrogenase of *Ralstonia eutropha* investigated by X-ray absorption spectroscopy: insights into O_2-tolerant H_2-cleavage, Biochemistry 50 (2011) 5858–5869.
[30] T. Goris, A.F. Wait, M. Saggu, J. Fritsch, N. Heidary, M. Stein, I. Zebger, F. Lendzian, F.A. Armstrong, B. Friedrich, O. Lenz, A unique iron–sulfur cluster is crucial for oxygen tolerance of a [NiFe]-hydrogenase, Nat. Chem. Biol. 7 (2011) 310–318.
[31] R.M. Evans, A. Parkin, M.M. Roessler, B.J. Murphy, H. Adamson, M.J. Lukey, F. Sargent, A. Volbeda, J.C. Fontecilla-Camps, F.A. Armstrong, Principles of sustained enzymatic hydrogen oxidation in the presence of oxygen — the crucial influence of high potential Fe–S clusters in the electron relay of [NiFe]-hydrogenases, J. Am. Chem. Soc. 135 (2013) 2694–2707.
[32] Z.J. Gu, J. Dong, C.B. Allan, S.B. Choudhury, R. Franco, J.J.G. Moura, J. LeGall, A.E. Przybyla, W. Roseboom, S.P.J. Albracht, M.J. Axley, R.A. Scott, M.J. Maroney, Structure of the Ni sites in hydrogenases by x-ray absorption spectroscopy. Species variation and the effects of redox poise, J. Am. Chem. Soc. 118 (1996) 11155–11165.
[33] T. Buhrke, S. Löscher, O. Lenz, E. Schlodder, I. Zebger, L.K. Andersen, P. Hildebrandt, W. Meyer-Klaucke, H. Dau, B. Friedrich, M. Haumann, Reduction of unusual iron–sulfur clusters in the H_2-sensing regulatory Ni–Fe hydrogenase from *Ralstonia eutropha* H16, J. Biol. Chem. 280 (2005) 19488–19495.
[34] T. Burgdorf, S. Löscher, P. Liebisch, E. Van der Linden, M. Galander, F. Lendzian, W. Meyer-Klaucke, S.P. Albracht, B. Friedrich, H. Dau, M. Haumann, Structural and oxidation-state changes at its nonstandard Ni–Fe site during activation of the NAD-reducing hydrogenase from *Ralstonia eutropha* detected by X-ray absorption, EPR, and FTIR spectroscopy, J. Am. Chem. Soc. 127 (2005) 576–592.
[35] W.W. Gu, L. Jacquamet, D.S. Patil, H.X. Wang, D.J. Evans, M.C. Smith, M. Millar, S. Koch, D.M. Eichhorn, M. Latimer, S.P. Cramer, Refinement of the nickel site structure in *Desulfovibrio gigas* hydrogenase using range-extended EXAFS spectroscopy, J. Inorg. Biochem. 93 (2003) 41–51.
[36] M.J. Lukey, A. Parkin, M.M. Roessler, B.J. Murphy, J. Harmer, T. Palmer, F. Sargent, F.A. Armstrong, How *Escherichia coli* is equipped to oxidize hydrogen under different redox conditions, J. Biol. Chem. 285 (2010) 3928–3938.
[37] K.S. Yoon, Y. Sakai, N. Tsukada, K. Fujisawa, H. Nishihara, Purification and biochemical characterization of a membrane-bound [NiFe]-hydrogenase from a hydrogen-oxidizing, lithotrophic bacterium, *Hydrogenophaga* sp. AH-24, FEMS Microbiol. Lett. 290 (2009) 114–120.
[38] O. Rüdiger, J.M. Abad, E.C. Hatchikian, V.M. Fernandez, A.L. De Lacey, Oriented immobilization of *Desulfovibrio gigas* hydrogenase onto carbon electrodes by covalent bonds for nonmediated oxidation of H_2, J. Am. Chem. Soc. 127 (2005) 16008–16009.
[39] S. Dementin, F. Leroux, L. Cournac, A.L. de Lacey, A. Volbeda, C. Legèr, B. Burlat, N. Martinez, S. Champ, L. Martin, O. Sanganas, M. Haumann, V.M. Fernandez, B. Guigliarelli, J.C. Fontecilla-Camps, M. Rousset, Introduction of methionines in the gas channel makes [NiFe] hydrogenase aero-tolerant, J. Am. Chem. Soc. 131 (2009) 10156–10164.
[40] M.E. DerVartanian, N.K. Menon, A.E. Przybyla, H.D. Peck Jr., D.V. DerVartanian, Electron paramagnetic resonance (EPR) studies on hydrogenase-1 (HYD1) purified from a mutant strain (AP6) of *Escherichia coli* enhanced in HYD1, Biochem. Biophys. Res. Commun. 227 (1996) 211–215.
[41] A.L. De Lacey, A. Pardo, V.M. Fernandez, S. Dementin, G. Adryanczyk-Perrier, E.C. Hatchikian, M. Rousset, FTIR spectroelectrochemical study of the activation and inactivation processes of [NiFe] hydrogenases: effects of solvent isotope replacement and site-directed mutagenesis, J. Biol. Inorg. Chem. 9 (2004) 636–642.
[42] Y. Nicolet, A.L. de Lacey, X. Vernede, V.M. Fernandez, E.C. Hatchikian, J.C. Fontecilla-Camps, Crystallographic and FTIR spectroscopic evidence of changes in Fe coordination upon reduction of the active site of the Fe-only hydrogenase from *Desulfovibrio desulfuricans*, J. Am. Chem. Soc. 123 (2001) 1596–1601.
[43] R. Klockenkämper, Total Reflection X-ray Fluorescence Analysis, Wiley-VCH, London, UK, 1996.
[44] H. Dau, P. Liebisch, M. Haumann, X-ray absorption spectroscopy to analyze nuclear geometry and electronic structure of biological metal centers — potential and questions examined with special focus on the tetra-nuclear manganese complex of oxygenic photosynthesis, Anal. Bioanal. Chem. 376 (2003) 562–583.
[45] H. Dau, P. Liebisch, M. Haumann, The structure of the manganese complex of photosystem II in its dark-stable S_1-state: EXAFS results in relation to recent crystallographic data, Phys. Chem. Chem. Phys. 6 (2004) 4781–4792.
[46] J.J. Rehr, J.J. Kas, F.D. Vila, M.P. Prange, K. Jorissen, Parameter-free calculations of X-ray spectra with FEFF9, Phys. Chem. Chem. Phys. 12 (2010) 5503–5513.
[47] C. Lambertz, P. Chernev, K. Klingan, N. Leidel, K.G.V. Sigfridsson, T. Happe, M. Haumann, Electronic and molecular structures of the active-site H-cluster in [FeFe]-hydrogenase determined by site-selective X-ray spectroscopy and quantum chemical calculations, Chem. Sci. 5 (2014) 1187–1203.
[48] S. Frielingsdorf, J. Fritsch, A. Schmidt, M. Hammer, J. Löwenstein, E. Siebert, V. Pelmenschikov, T. Jaenicke, J. Kalms, Y. Rippers, F. Lendzian, I. Zebger, C. Teutloff, M. Kaupp, R. Bittl, P. Hildebrandt, B. Friedrich, O. Lenz, P. Scheerer, Reversible

[4Fe–3S] cluster morphing in an O_2-tolerant [NiFe] hydrogenase, Nat. Chem. Biol. 10 (2014) 378–385.
[49] S. Löscher, T. Burgdorf, I. Zebger, P. Hildebrandt, H. Dau, B. Friedrich, M. Haumann, Bias from H_2 cleavage to production and coordination changes at the Ni–Fe active site in the NAD^+-reducing hydrogenase from *Ralstonia eutropha*, Biochemistry 45 (2006) 11658–11665.
[50] H. Ogata, S. Hirota, A. Nakahara, H. Komori, N. Shibata, T. Kato, K. Kano, Y. Higuchi, Activation process of [NiFe] hydrogenase elucidated by high-resolution X-ray analyses: conversion of the ready to the unready state, Structure 13 (2005) 1635–1642.
[51] O. Trofanchuk, M. Stein, C. Gessner, F. Lendzian, Y. Higuchi, W. Lubitz, Single crystal EPR studies of the oxidized active site of [NiFe] hydrogenase from Desulfovibrio vulgaris Miyazaki F. J. Biol. Inorg. Chem. 5 (2000) 36–44.
[52] A. Volbeda, E. Garcin, C. Piras, A.L. deLacey, V.M. Fernandez, E.C. Hatchikian, M. Frey, J.C. FontecillaCamps, Structure of the [NiFe] hydrogenase active site: evidence for biologically uncommon Fe ligands, J. Am. Chem. Soc. 118 (1996) 12989–12996.
[53] G. Davidson, S.B. Choudhury, Z. Gu, K. Bose, W. Roseboom, S.P. Albracht, M.J. Maroney, Structural examination of the nickel site in *Chromatium vinosum* hydrogenase: redox state oscillations and structural changes accompanying reductive activation and CO binding, Biochemistry 39 (2000) 7468–7479.
[54] M.E. Pandelia, W. Nitschke, P. Infossi, M.T. Giudici-Orticoni, E. Bill, W. Lubitz, Characterization of a unique [FeS] cluster in the electron transfer chain of the oxygen tolerant [NiFe] hydrogenase from *Aquifex aeolicus*, Proc. Natl. Acad. Sci. U. S. A. 108 (2011) 6097–6102.
[55] M.E. Pandelia, P. Infossi, M.T. Giudici-Orticoni, W. Lubitz, The oxygen-tolerant hydrogenase I from *Aquifex aeolicus* weakly interacts with carbon monoxide: an electrochemical and time-resolved FTIR study, Biochemistry 49 (2010) 8873–8881.
[56] M. Saggu, M. Ludwig, B. Friedrich, P. Hildebrandt, R. Bittl, F. Lendzian, O. Lenz, I. Zebger, Impact of amino acid substitutions near the catalytic site on the spectral properties of an O-2-tolerant membrane-bound [NiFe] hydrogenase, ChemPhysChem 11 (2010) 1215–1224.
[57] F. Leroux, S. Dementin, B. Burlatt, L. Cournac, A. Volbeda, S. Champ, L. Martin, B. Guigliarelli, P. Bertrand, J. Fontecilla-Camps, M. Rousset, C. Legèr, Experimental approaches to kinetics of gas diffusion in hydrogenase, Proc. Natl. Acad. Sci. U. S. A. 105 (2008) 11188–11193.
[58] A. Abou Hamdan, B. Burlat, O. Gutierrez-Sanz, P.P. Liebgott, C. Baffert, A.L. De Lacey, M. Rousset, B. Guigliarelli, C. Leger, S. Dementin, O2-independent formation of the inactive states of NiFe hydrogenase, Nat. Chem. Biol. 9 (2013) 15–17.
[59] M. Carepo, D.L. Tierney, C.D. Brondino, T.C. Yang, A. Pamplona, J. Telser, I. Moura, J.J.G. Moura, B.M. Hoffman, O-17 ENDOR detection of a solvent-derived Ni-(OHx)-Fe bridge that is lost upon activation of the hydrogenase from *Desulfovibrio gigas*, J. Am. Chem. Soc. 124 (2002) 281–286.
[60] J.W. van der Zwaan, J.M. Coremans, E.C. Bouwens, S.P. Albracht, Effect of $^{17}O_2$ and ^{13}CO on EPR spectra of nickel in hydrogenase from *Chromatium vinosum*, Biochim. Biophys. Acta 1041 (1990) 101–110.
[61] B. Bleijlevens, F.A. van Broekhuizen, A.L. De Lacey, W. Roseboom, V.M. Fernandez, S.P.J. Albracht, The activation of the [NiFe]-hydrogenase from *Allochromatium vinosum*. An infrared spectro-electrochemical study, J. Biol. Inorg. Chem. 9 (2004) 743–752.
[62] K.A. Vincent, J.A. Cracknell, O. Lenz, I. Zebger, B. Friedrich, F.A. Armstrong, Electrocatalytic hydrogen oxidation by an enzyme at high carbon monoxide or oxygen levels, Proc. Natl. Acad. Sci. U. S. A. 102 (2005) 16951–16954.
[63] H. Ogata, Y. Mizoguchi, N. Mizuno, K. Miki, S. Adachi, N. Yasuoka, T. Yagi, O. Yamauchi, S. Hirota, Y. Higuchi, Structural studies of the carbon monoxide complex of [NiFe]hydrogenase from *Desulfovibrio vulgaris* Miyazaki F: suggestion for the initial activation site for dihydrogen, J. Am. Chem. Soc. 124 (2002) 11628–11635.
[64] P.P. Liebgott, A.L. de Lacey, B. Burlat, L. Cournac, P. Richaud, M. Brugna, V.M. Fernandez, B. Guigliarelli, M. Rousset, C. Leger, S. Dementin, Original design of an oxygen-tolerant [NiFe] hydrogenase: major effect of a valine-to-cysteine mutation near the active site, J. Am. Chem. Soc. 133 (2011) 986–997.
[65] A. Parkin, G. Goldet, C. Cavazza, J.C. Fontecilla-Camps, F.A. Armstrong, The difference a Se makes? Oxygen-tolerant hydrogen production by the [NiFeSe]-hydrogenase from *Desulfomicrobium baculatum*, J. Am. Chem. Soc. 130 (2008) 13410–13416.
[66] A. Volbeda, C. Darnault, A. Parkin, F. Sargent, F.A. Armstrong, J.C. Fontecilla-Camps, Crystal structure of the O_2-tolerant membrane-bound hydrogenase 1 from *Escherichia coli* in complex with its cognate cytochrome b, Structure 21 (2013) 184–190.